ACS Sustainable Chemistry & Engineering

Research Article

pubs.acs.org/journal/ascecg

Dialysis-Free and in Situ Doping Synthesis of Polypyrrole@Cellulose Nanowhiskers Nanohybrid for Preparation of Conductive Nanocomposites with Enhanced Properties

Xinxing Zhang,*,† Xiaodong Wu,† Canhui Lu,* and Zehang Zhou

State Key Laboratory of Polymer Materials Engineering, Polymer Research Institute of Sichuan University, Chengdu 610065, China

Supporting Information

ABSTRACT: The separation of cellulose nanowhiskers (CNs) from hydrolysis acid and the harmless disposal of the residual hydrolysis acid are two main obstacles that hinder the large-scale production of CNs and CNs based nanocomposites. In this work, the hydrolysis products of CNs without further separation were used as the starting materials for preparation of a CNs supported polypyrrole (PPy@CNs) nanohybrid. During this one-pot synthesis process, the residual hydrolysis acid acted as a doping agent for the synthesized PPy, endowing PPy@CNs nanohybrid with electrical conductivity. Interestingly, the PPy@CNs nanohybrid could be easily isolated from the polymerization products due to the decreased surface charge. Meanwhile, the PPy@CNs nanohybrid showed good suspension stability in alkaline natural rubber (NR) latex, which facilitated the construction of continuous PPy@CNs conductive network in the NR matrix. This PPy@CNs filled NR nanocomposite showed significant improvement in electrical conductivity and mechanical properties when compared with neat PPy/NR composites, and exhibited similar performance to that of PPy@CNs-0 (CNs was isolated by dialysis and virgin doping agent was used) filled NR nanocomposites. The straightforwardness and sustainability of this dialysis-free and in situ doping synthesis of the PPy@CNs nanohybrid should significantly facilitate the scalable fabrication and application of CNs based conductive nanocomposites with high performance.

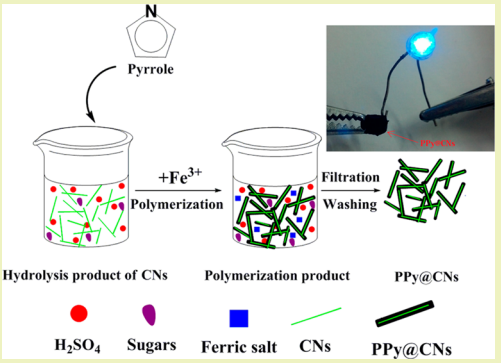

KEYWORDS: *Cellulose nanowhiskers, acid hydrolysis, polypyrrole, in situ doping, conductive nanocomposites*

INTRODUCTION

Cellulose is an almost inexhaustible raw material derived from nature with a biomass production of 1.5×10^{12} tons per year.[1−3] Cellulose nanowhiskers (CNs), which are derived from natural cellulose fibers by controlled acid hydrolysis, have attracted much attention because of their unique properties:[4,5] enriched surface active groups, high aspect ratio and specific surface area, good water dispersibility, strong yet lightweight, and most importantly, environmental sustainability. Hence, CNs are widely used in numerous applications such as polymer reinforcement, enzyme immobilization, drug delivery, catalyst support, etc.[6−9]

Acid hydrolysis of bulk cellulose to produce CNs was developed in the 1950s,[10] which is the most utilized and viable process for producing CNs due to the controllable and convenient treatment. During the controlled acid hydrolysis process, the amorphous region of bulk cellulose is highly susceptible to hydrolysis and hydrolyzed into soluble sugars with small molecular weight, leaving the crystalline regions intact, i.e., CNs with diameters of 5−20 nm and lengths of around 100−400 nm. Then CNs are isolated from the waste hydrolysate by centrifugation and dialysis to remove the soluble sugars and residual acids. However, this dialysis process is time-consuming (usually several days) and water-consuming. Furthermore, the dialysis membranes are very expensive, which drastically increases production cost. On the other hand, the harmless disposal of the residual hydrolysis acid is also an urgent issue to address. Hence, these drawbacks significantly restrict the industrial-scale production and application of CNs and CNs based nanocomposites.

In recent years, composite materials of nanocellulose and conductive polymers, such as polypyrrole (PPy), polyaniline (PANI), and polyrhodanine, have exhibited potential applications as energy-storage devices,[11−15] biomaterials,[16] conducting films,[17] and optical pH indicators.[18] The poor mechanical strength, processability and dispersibility as well as the low special surface area of these conductive polymers could be significantly improved by incorporation of renewable and biodegradable nanocellulose. Furthermore, our previous work[19] indicated that CNs could act as a biotemplate and direct the growth of PANI into rod-like PANI@CNs nanohybrid with high aspect ratio and good dispersity, which enabled the fabrication of a 3D hierarchical multiscale conductive structure in a natural rubber (NR) matrix. Unfortunately, the high-cost,

Received: December 31, 2014
Revised: March 1, 2015
Published: March 4, 2015

DOI: 10.1021/sc500853m
ACS Sustainable Chem. Eng. 2015, 3, 675−682

time-consuming and environmentally harmful process of producing CNs is the main barrier in the practical application of CNs based conductive nanocomposites.

To realize the economically and ecologically feasible approach to CNs based conductive nanohybrids, we made the first attempt, to the best of our knowledge, to develop a dialysis-free and in situ doping synthesis method of a CNs supported PPy (PPy@CNs) nanohybrid, which avoided the time-consuming and water-consuming dialysis process of CNs. The synthesized PPy@CNs was in situ doped by the residual hydrolysis acid during the synthesis process, giving the PPy@CNs nanohybrid electrical conductivity. Interestingly, the PPy@CNs nanohybrid could be easily isolated from the polymerization products due to the decreased surface charge, and showed excellent suspension stability in alkaline NR latex, which facilitated the construction of continuous PPy@CNs conductive network in NR matrix. The objective of this study is to open up new possibilities for the sustainable, low-cost and scalable approach to PPy@CNs conductive nanohybrid, which would be very promising for the large scale fabrication and application of CNs based conductive nanocomposites with high performance.

MATERIALS AND METHODS

Materials. Analytical grade ferric chloride hexahydrate ($FeCl_3 \cdot 6H_2O$, ≥99%), sulfuric acid (H_2SO_4, 95−98%), ammonium hydroxide ($NH_3 \cdot H_2O$, 25−28%), stearic acid (≥99.0%), OP emulsifier-10 (≥99.0%), and zinc oxide (≥98.0%) were all purchased from Chendu Kelong Chemical Reagent Company (China) and used without further purification. Pyrrole (≥98.0%) was purchased from Shanghai Kefeng industrial Co., Ltd. (China). The NR latex (solid content: 58 wt %) was provided by Chengdu Xinyuanding Co., Ltd. (China). Medical purified cotton was obtained from Xuzhou Health Factory Co., Ltd. (China). Vulcanization agent sulfur (≥98%) and accelerator *N*-cyclohexyl-2-benzothiazolesulfenamide (CBS, active content: ≥80%) was purchased from Weihai Tianyu New Mstar Technology Co., Ltd. (China).

Dialysis-Free and in Situ Doping Preparation of PPy@CNs Nanohybrid. Acid hydrolysis of bulk cellulose to produce CNs was based on our previous studies.[19] Medical purified cotton (11.5 g) was mixed with sulfuric acid solution (200 mL, 64 wt %) and the mixture was stirred vigorously at 45 °C for 45 min. After hydrolysis, the hydrolysis product was immediately diluted 6.4 times to stop the hydrolysis. The hydrolysis product was centrifuged at 4000 rpm for 5 min, and half of the supernatant hydrolysate was separated for other use. 640 mL of deionized water was added into the hydrolysis product to adjust the sulfuric acid concentration to 0.5 M. Then 24.1 g of pyrrole (0.355 mol) was dissolved in the remaining hydrolysis product (containing CNs, soluble sugars, residual acid), and the mixture was stirred evenly in ice−water for 1 h. Whereafter, 48.4 g of $FeCl_3 \cdot 6H_2O$ (0.179 mol) was added into the mixture to initiate the polymerization. The polymerization proceeded in ice−water for 2 h. The obtained product was filtered and washed several times with distilled water to remove the remaining reagents. The resulted PPy@CNs nanohybrid was diluted to 1280 mL again. The solid content of the PPy@CNs nanohybrid suspension was measured 5 times and the mean value was 0.78 ± 0.05 wt %. The mass ratio of PPy/CNs in the PPy@CNs nanohybrid was about 1:1 by measuring the neat CNs solid content via dialysis.

Conventional Preparation of PPy@CNs Nanohybrid and Neat PPy. The producing process of CNs was the same as above. However, the hydrolysis product was centrifuged and washed with deionized water for three times. Then the centrifuged hydrolysis product was dialyzed with regenerated cellulose membrane (molecular weight cut off of 8000−14 000) to remove the soluble sugar and residual acid by replacing the dialysate repeatedly. The result was monitored by checking the neutrality of the dialyzate, which usually proceeded for several days. Whereafter, 62.72 g of virgin H_2SO_4 (0.64 mol) and 24.1 g of pyrrole (0.355 mol) were added into the CNs suspension. After magnetic stirring in ice−water for 1 h, 48.4 g of $FeCl_3 \cdot 6H_2O$ (0.179 mol) was added and the polymerization proceeded in ice−water for 2 h. The aftertreatment was as same as mentioned above. This traditionally synthesized dialyzed CNs supported PPy nanohybrid doped with virgin H_2SO_4 is marked as PPy@CNs-0. Neat PPy was synthesized in the absence of CNs, and all other conditions were in accordance with the PPy@CNs-0 nanohybrid.

Preparation of PPy@CNs/NR Nanocomposites. In the preparation of PPy@CNs/NR nanocomposites, the obtained PPy@CNs nanohybrid was filtered and washed with 1 M $NH_3 \cdot H_2O$ and deionized water to dedope the doping H_2SO_4 in PPy@CNs nanohybrid, which can cause the coagulation of NR latex. Then the desired amount of PPy@CNs nanohybrids suspension was diluted to 500 mL (the pH value was adjusted to 9 with 1 M $NH_3 \cdot H_2O$) and sonicated for 10 min to disperse the aggregation. Simultaneously, 8.6 g of NR latex was diluted to 250 mL and stirred for a while. Then the 500 mL sonicated PPy@CNs nanohybrid suspension and 250 mL of NR latex, as well as an aqueous suspension containing cross-linking agent sulfur and other additives (the experimental vulcanization formula is given in the Supporting Information), were mixed together to form a homogeneous mixture. The final mixture was coagulated by adding 150 mL of the waste hydrolysate containing residual H_2SO_4 centrifuged from the hydrolysis product. In this coagulating process, the dedoped PPy on CNs was doped again by the residual H_2SO_4 simultaneously, endowing PPy@CNs nanohybrid with electrical conductivity. After filtering, the solid mixture was soaked in renewed distilled water to remove the residual H_2SO_4 and finally dried at 60 °C for 12 h. The dried composites were cut into pieces, molded using compression molding and vulcanized at a temperature of 150 °C and a pressure of 10 MPa for 5 min. The PPy@CNs-0/NR and PPy/NR composites were prepared according to the same procedure of the aforementioned PPy@CNs/NR nanocomposites except for the use of virgin H_2SO_4 as the coagulating and doping agent.

CHARACTERIZATION

The ζ-potential (ZP) values of CNs (0.019 wt %, pH = 6.5), PPy@CNs nanohybrid (0.039 wt %, pH = 7.2), dedoped PPy@CNs nanohybrid (0.039 wt %, pH = 7.4), and dedoped PPy@CNs nanohybrid (0.039 wt %, pH = 9.6) suspensions in water were measured using a Zetasizer nano-ZS instrument (Malvern, UK).

Transmission electron microscopy (TEM) was performed using a transmission electron microscope (JEOL JEM-100CX, Japan). Diluted CNs (0.05 wt %) and PPy@CNs nanohybrid (0.1 wt %) aqueous suspensions were sonicated for 30 min to disperse the aggregation. The well dispersed CNs and PPy@CNs nanohybrid suspensions were dropped on a copper grid for 5 min, and the excess solution in the droplet was blotted with filter paper. CNs were negatively stained with 1.5 wt % aqueous uranyl acetate solution for imaging purposes. The diameter of pristine CNs was measured using Image-J software, and at least 50 particles from different TEM images were analyzed.

For Fourier transform infrared spectroscopy (FT-IR) studies, CNs, neat PPy, and PPy@CNs nanohybrid suspensions were freeze-dried and then dried at 60 °C in air-circulating oven for 12 h. FT-IR analysis was conducted using a Nicolet 6700 spectrophotometer (USA). The powdered samples of CNs, neat PPy, and PPy@CNs nanohybrid were mixed with KBr to produce tablets for FT-IR measurement. The spectra were recorded from 4000 to 400 cm^{-1} at a resolution of 2 cm^{-1}.

For UV−vis measurement, neat PPy and PPy@CNs nanohybrid suspensions (PPy content: 0.005 wt %, pH =

DOI: 10.1021/sc500853m
ACS Sustainable Chem. Eng. 2015, 3, 675−682

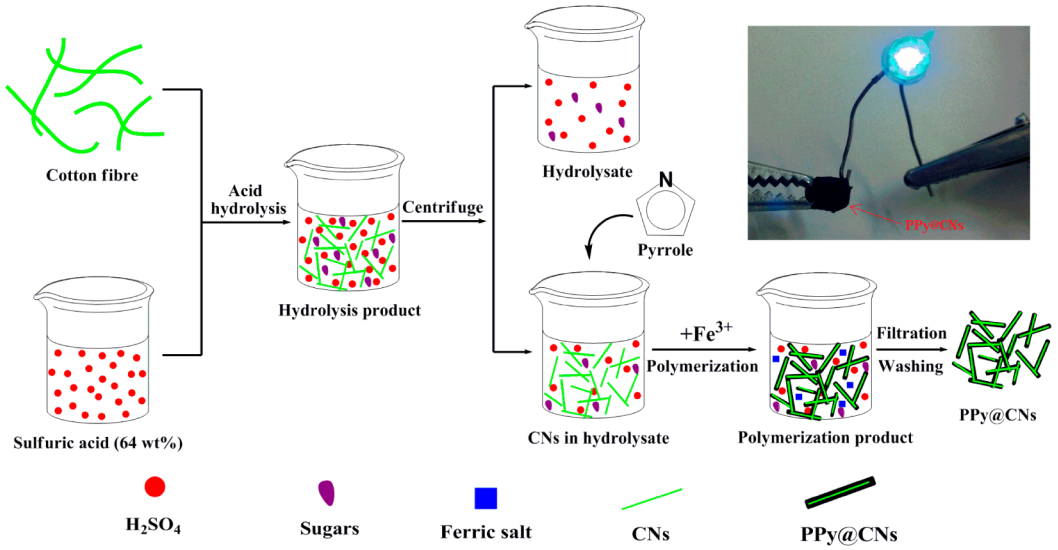

Figure 1. Schematic illustration for the dialysis-free and in situ doping synthesis of conductive PPy@CNs nanohybrid (the inset shows a PPy@CNs nanohybrid tablet light up an LED device).

9.6) were sonicated for 30 min to disperse the aggregation. The well dispersed PPy and PPy@CNs nanohybrid suspension was put into a quartz cuvette with an optical path of 1 cm. The measurement was conducted at room temperature by Shimadzu UVmini-1240 spectrophotometer.

An optical microscope with a digital camera (UB 200i, Chongqing UOP Photoelectric Technology Co., Ltd. China) was used to investigate the dispersion state and microstructures of the neat PPy and PPy@CNs nanohybrids. The suspension was dropped on a glass slide and covered with a coverslip. Then the samples were dried and observed.

Preparation of drop-cast sample of PPy@CNs/NR for TEM observation: 14.1 g of sonicated PPy@CNs nanohybrid suspension, and 0.86 g of NR latex (58 wt %) were mixed and diluted to 550 mL. The mixture of PPy@CNs nanohybrid and NR latex was stirred and sonicated adequately for uniform mixing. The mixture was put on the copper grid and the water was evaporated. The final sample was observed using a transmission electron microscope (JEOL JEM-100CX, Japan).

The electric conductivity of all samples was measured on undeformed samples by a two-point measurement with a resistance meter (UT61, Uni-Trend, China) for $R \leq 2 \times 10^8$ Ω or using a ZC36 high resistance instrument for $R > 2 \times 10^8$ Ω. Rectangle strip samples (40 × 10 × 1 mm) or square samples (100 × 100 × 1 mm) were used for electrical measurement. Five specimens were measured for each sample to achieve an average value. The measured volume resistance (Ω), R_v, was converted to volume resistivity, ρ_v, according to ASTM D4496 and D257 using the formula

$$\rho_v = R_v \frac{A}{t}$$

where A is effective area of the measuring electrode (m^2) and t is specimen thickness (m).

Mechanical properties measurement was conducted on a versatile testing machine (ASTM D412-80) at room temperature. The rectangle specimens (40 × 10 × 1 mm) were stretched at a crosshead rate of 100 mm/min. Five specimens were measured for each sample to achieve an average value.

RESULTS AND DISCUSSION

To better understand the dialysis-free and in situ doping synthesis of the PPy@CNs nanohybrid, the entire experimental process flow is schematically illustrated in Figure 1. Cellulose fibers were hydrolyzed by 64 wt % H_2SO_4, yielding a hydrolysis product consisting of CNs, soluble sugars, and residual acid. A portion of hydrolysate was separated by centrifugation for other use. The remaining hydrolysis product was used without further separation as the starting materials for the preparation of PPy@CNs nanohybrid, based on that the soluble sugars had no significant effect on polymerization of pyrrole. The polymerization of pyrrole was initiated with pyrrole monomer and ferric trichloride added into the hydrolysis product, and the generated PPy was deposited on CNs, yielding PPy@CNs nanohybrid. Meanwhile, the synthesized PPy@CNs nanohybrid was in situ doped by the residual hydrolysis acid, endowing the PPy@CNs nanohybrid electrical conductivity. Then PPy@CNs nanohybrid could be easily separated from the polymerization product by filtration and washing. The separated PPy@CNs nanohybrid was dried in a drying oven at 60 °C for 12 h, obtaining a PPy@CNs tablet with low electrical resistance (hundreds Ω). A blue LED light was connected with the PPy@CNs tablet using a metal line to form a conductive network. The lighting LED is illuminated by a 9.0 V battery (Figure S1 of the Supporting Information), indicating the desired electrical conductivity of this synthesized PPy@CNs nanohybrid. This facile, inexpensive, and eco-friendly approach to a PPy@CNs nanohybrid not only avoided the time-consuming and water-consuming dialysis process of CNs but also utilized the residual hydrolysis acid as doping agent, which might dramatically reduce the production cost of PPy@CNs and widely extend its applications.

ζ-Potential (ZP) is a crucial parameter of stability for suspension systems. For a stable suspension solely stabilized by electrostatic repulsion, a ζ-potential of ≥+30 mV or ≤−30 mV is necessary.[20] The ζ-potential values as well as the suspension performance of CNs and PPy@CNs nanohybrid are given in Figure 2. In neutral conditions (pH around 7.0), the ζ-potential of CNs was measured to be −37.3 mV, which is much higher than that of the PPy@CNs nanohybrid (−16.7 mV). The CNs

DOI: 10.1021/sc500853m
ACS Sustainable Chem. Eng. 2015, 3, 675−682

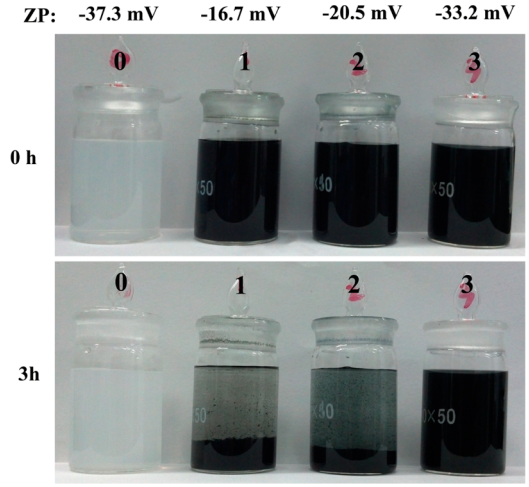

Figure 2. Digital pictures along with ζ-potential of CNs (0, pH = 6.5), PPy@CNs (1, pH = 7.2), dedoped PPy@CNs (2, pH = 7.4), and dedoped PPy@CNs (3, pH = 9.6) nanohybrid aqueous suspensions before and after standing for 3 h.

suspension remained stable after left standing for 3 h. This might be attributed to the sulfate ester groups on CNs, which could electrostatically stabilize CNs. Although, the PPy@CNs nanohybrid suspension showed significant sedimentation because of the coating of PPy on CNs. These indicate that CNs exhibit better suspension stability than the PPy@CNs nanohybrid. The excellent stability and nanometric dispersity of CNs make them difficult to be separated from the hydrolysis product, except for the time-consuming, water-consuming, and costly dialysis process. However, after CNs were coated with PPy, the PPy@CNs nanohybrid exhibited relative poor suspension stability at a neutral or acidic condition and settled through aggregation, which makes it easier to be separated by filtration due to the decreased surface charge.

In addition, the suspension property of the dedoped PPy@CNs nanohybrid with different pH values was also evaluated. In neutral conditions (pH = 7.4), the dedoped PPy@CNs nanohybrid exhibited a ζ-potential of −20.5 mV and settled through aggregation. However, in alkaline conditions (pH = 9.6), the dedoped PPy@CNs nanohybrid exhibited a high ζ-potential (−33.2 mV) and excellent stability (no noticeable sedimentation was observed after standing for 3 h). This might be attributed to the insertion or aggregation of OH^- on the surface of the PPy@CNs nanohybrid in alkaline conditions. Moreover, the PPy@CNs-0 nanohybrid prepared via conventional routes (CNs was isolated from hydrolysate by dialysis and virgin doping acid was used for PPy@CNs-0 nanohybrid) exhibited a similar suspension performance and ζ-potential (Figure S2 of the Supporting Information) as the PPy@CNs nanohybrid. The good suspension stability of the PPy@CNs nanohybrid in alkaline conditions might make it very suitable for homogeneous dispersion in alkaline NR latex and fabrication of PPy@CNs/NR nanocomposites.

TEM observation was employed to investigate the microstructures of pristine CNs and the PPy@CNs nanohybrid. In Figure 3a, needle-like CNs with a length of 132 ± 35 nm and width of 8.2 ± 2.1 nm could be clearly observed. After the polymerization of the pyrrole monomer, as shown in Figure 3b, it can be found that a nodular structure of PPy was deposited on the surface of CNs, forming a continuous nanosheath structure with a high aspect ratio. Large scale aggregation of

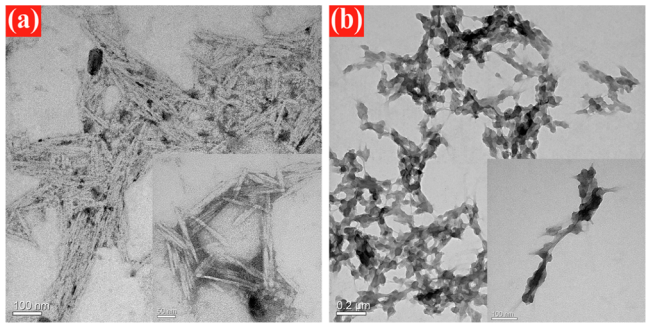

Figure 3. TEM images of CNs (a, scale bar: 100 nm for low and 50 nm for high magnification) and PPy@CNs nanohybrid (b, scale bar: 200 nm for low and 100 nm for high magnification).

PPy was not observed. This demonstrates that CNs can act as a good template for the polymerization of a pyrrole monomer. Moreover, the PPy@CNs-0 nanohybrid prepared via conventional routes exhibited a similar morphology (Figure S3 of the Supporting Information) as that of the PPy@CNs nanohybrid. The hydrogen bonds between imine groups of PPy and hydroxyl groups of CNs might serve as a traction force to assist the growing of the continuous nanosheath of PPy on CNs and prevented the formation of large scale PPy aggregation.[21]

FT-IR analysis of CNs, neat PPy, and PPy@CNs nanohybrid was carried out to study their chemical structures. As shown in Figure 4, CNs present characteristic bands around 3417 and

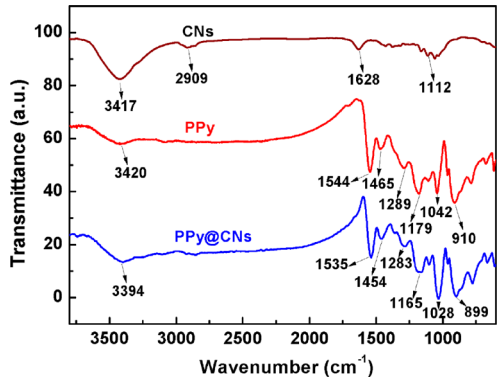

Figure 4. FT-IR spectra of CNs, neat PPy, and PPy@CNs nanohybrid.

2909 cm^{-1}, which are attributed to the O—H stretching and C—H stretching in cellulose, respectively. The band at 1628 cm^{-1} is ascribed to the H—O—H bending of the absorbed water. The three small bands around 1112 cm^{-1} are due to the C—O—C pyranose ring skeletal vibration.[22] The characteristic bands of neat PPy can also be observed clearly. The bands around 3420 and 1544 cm^{-1} are responsible for the N—H stretching vibration and C═C ring stretching of the quinonoid structure in PPy. The band at 1465 cm^{-1} is attributed to C—N stretching vibration in the pyrrole ring. Additionally, bands at 1289, 1179, and 1042 cm^{-1} are ascribed to C—H on-plane vibration, and the band at 910 cm^{-1} is for C—H out-of-plane vibration.[23] The PPy@CNs nanohybrid exhibited a similar spectrum as that of neat PPy, but all major peaks for PPy@CNs shifted to lower wavenumbers, suggesting the existence of the interaction between PPy and CNs.[24−26]

For most intrinsic conductive polymers, the poor dispersibility and processability, which are due to the agglomeration resulting from strong intermolecular interactions (π−π

DOI: 10.1021/sc500853m
ACS Sustainable Chem. Eng. 2015, 3, 675−682

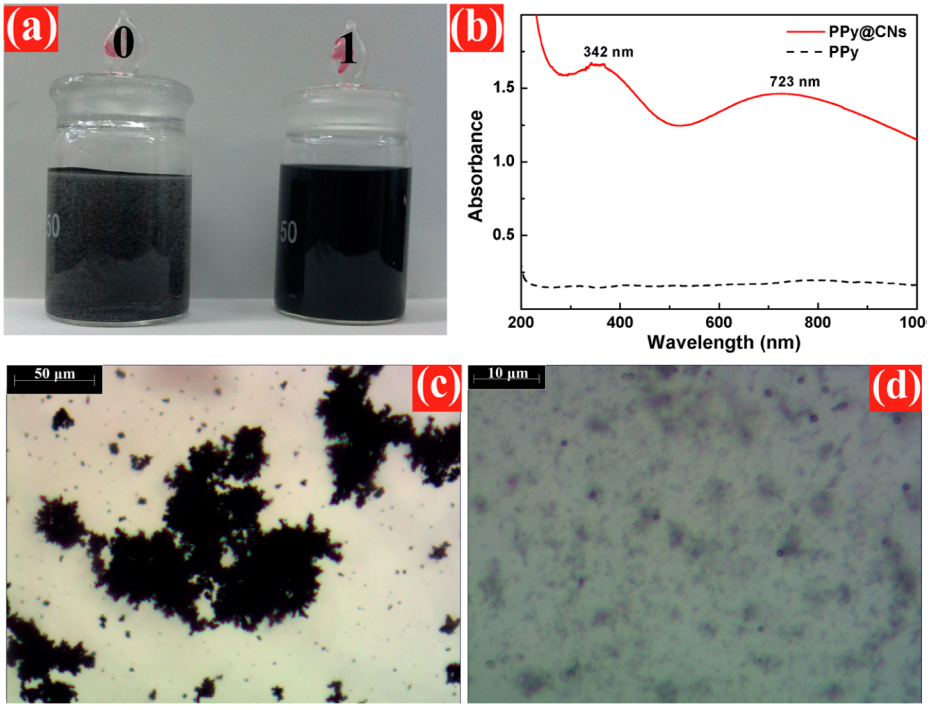

Figure 5. Digital picture (a) and UV−vis spectra (b) of neat PPy (0) and PPy@CNs nanohybrid (1) suspension; optical microscope images of neat PPy (c, scale bar: 50 μm) and PPy@CNs nanohybrid (d, scale bar: 10 μm).

interaction, hydrogen bond, and so on), severely hinder their practical applications. As shown in Figure 5a,c, large scale agglomeration of PPy with dozens of micrometers could be clearly observed in PPy aqueous suspension (pH = 9.6), whereas the PPy@CNs nanohybrid is homogeneously dispersed (pH = 9.6) and no visible particles are observed (Figure 5a,d). Furthermore, the absorption peak in UV−vis spectra of neat PPy suspension is much weaker than that of the PPy@CNs nanohybrid (Figure 5b) at the same PPy concentration (0.005 wt %), because PPy was poorly dispersed in water and usually precipitated out as large aggregation. These results confirm that the dispersibility of PPy could be significantly improved by the incorporation of renewable and biodegradable CNs. In addition, the PPy@CNs nanohybrid shows two absorption bands around 342 and 723 nm in the UV−vis spectrum. The first band around 342 nm is due to the $\pi-\pi^*$ interband transition and the second broad band around 723 nm is assigned to the polaron and bipolaron band transition of PPy,[27] indicating the successful synthesis of PPy on CNs. Thus, PPy@CNs nanohybrid with a high aspect ratio was successfully synthesized by incorporation of CNs using a dialysis-free and in situ doping route. Compared with neat PPy, this PPy@CNs nanohybrid exhibited a good and adjustable suspension property, which makes it more suitable and effective to fabricate PPy based conductive nanocomposites.

To evaluate the feasibility of this PPy@CNs nanohybrid in construction of conductive polymer nanocomposites, we prepared PPy@CNs/NR nanocomposite by mixing the PPy@CNs nanohybrid and NR latex. The morphology of PPy@CNs/NR nanocomposite was characterized by TEM observation. As shown in Figure 6, the PPy@CNs nanohybrid is located in the interstitial space between the NR latex particles and formed a continuous network, which benefited from the good suspension property and high aspect ratio of the PPy@CNs nanohybrid. This continuous network structure was

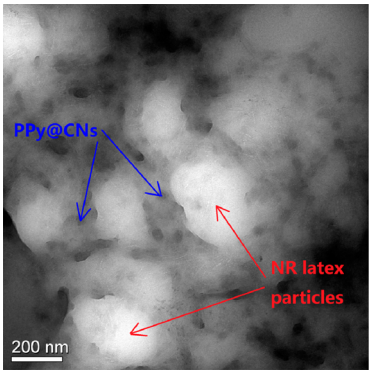

Figure 6. TEM image of PPy@CNs/NR nanocomposite prepared by self-assembly of PPy@CNs nanohybrid and NR latex particles (scale bar: 200 nm).

expected to realize the enhancement of electrical conductivity as well as mechanical properties of the PPy@CNs/NR nanocomposites. A detailed investigation and formation mechanism of the continuous conductive network in the NR matrix constructed by a CNs supported conductive polymer have been reported in our previous work.[19]

To achieve higher conductivity at the same PPy content, we expected that all the PPy can participate in the fabrication of a continuously conductive network in a NR matrix. Unfortunately, severe agglomeration was observed in the neat PPy sample because of its poor suspension stability, which made it difficult to connect with each other and form conductive networks.[19] However, a continuous network structure of PPy@CNs nanohybrid (Figure 6) could be formed by incorporation of CNs due to the remarkably enhanced stability in alkaline NR latex. As a result, compared with PPy/NR, significant electrical conductivity enhancement is observed for all PPy@CNs/NR samples (Figure 7). For example, the electrical conductivity of

DOI: 10.1021/sc500853m
ACS Sustainable Chem. Eng. 2015, 3, 675−682

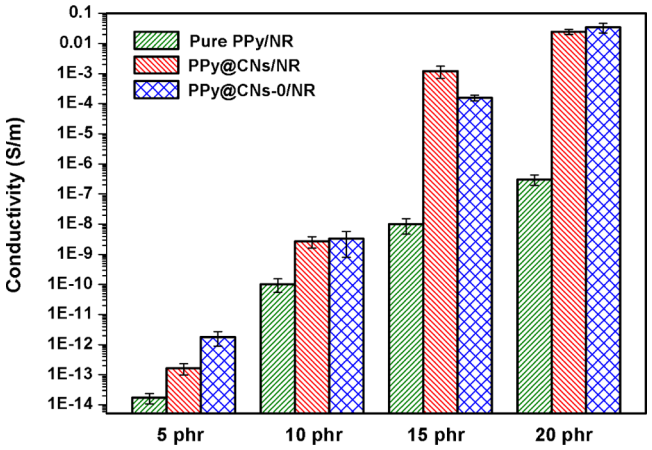

Figure 7. Electrical conductivity of PPy/NR, PPy@CNs/NR, and PPy@CNs-0/NR nanocomposites with different PPy content.

the PPy/NR composite containing 15 phr PPy is 9.98×10^{-9} S/m, whereas for PPy@CNs/NR nanocomposites at the same loading fraction of PPy, it reaches 1.22×10^{-3} S/m, showing a significant enhancement of about 5 orders of magnitude. This enhancement was benefited from the good suspension property and high aspect ratio of the PPy@CNs nanohybrid. Besides, we compared the electrical conductivity of the PPy@CNs/NR nanocomposites made from this synthesized PPy@CNs nanohybrid and PPy@CNs-0/NR nanocomposites made from the PPy@CNs-0 nanohybrid via conventional routes (CNs was isolated from hydrolysate by dialysis and virgin doping acid was used for the PPy@CNs-0 nanohybrid). The results showed that PPy@CNs/NR and PPy@CNs-0/NR nanocomposites exhibited similar electrical conductivities, indicating the same effectiveness of PPy@CNs and PPy@CNs-0 in fabrication of conductive composites.

The size, morphology, and dispersion state of conductive fillers have significant effects on the mechanical properties of conductive composites. Figure 8a presents the stress−strain curves of the PPy@CNs/NR nanocomposites with different PPy content. An obvious strain hardening phenomenon (i.e., increase in tensile strength associated with increasing strain) is observed in these stress−strain curves. This might be attributed to that the PPy@CNs nanohybrid was expected to be increasingly aligned along the tensile direction during sample elongation, and thus they were able to carry a larger share of the load exerted on the samples.[28] In addition, there is a remarkable increase in the tensile stress and Young's modulus associated with increasing PPy loading. However, elongation at break reaches to the highest value with 10 phr PPy, and then experiences a decrease with increased PPy loading, which has been also reported by other researchers.[28,29]

Besides, we compared the mechanical properties of PPy/NR, PPy@CNs/NR, and PPy@CNs-0/NR nanocomposites with different PPy content. As shown in Figure 8b−d, almost all PPy@CNs/NR samples exhibit higher tensile stress, Young's modulus, and elongation at break than that of neat PPy/NR composites, confirming the effective enhancement of mechanical properties by incorporation of renewable and biodegradable CNs. On the other hand, the mechanical properties of PPy@CNs/NR nanocomposites were comparable to that of PPy@CNs-0/NR nanocomposites. This superior (straightforward, green, cost-effective, and scalable) approach to PPy@CNs/NR

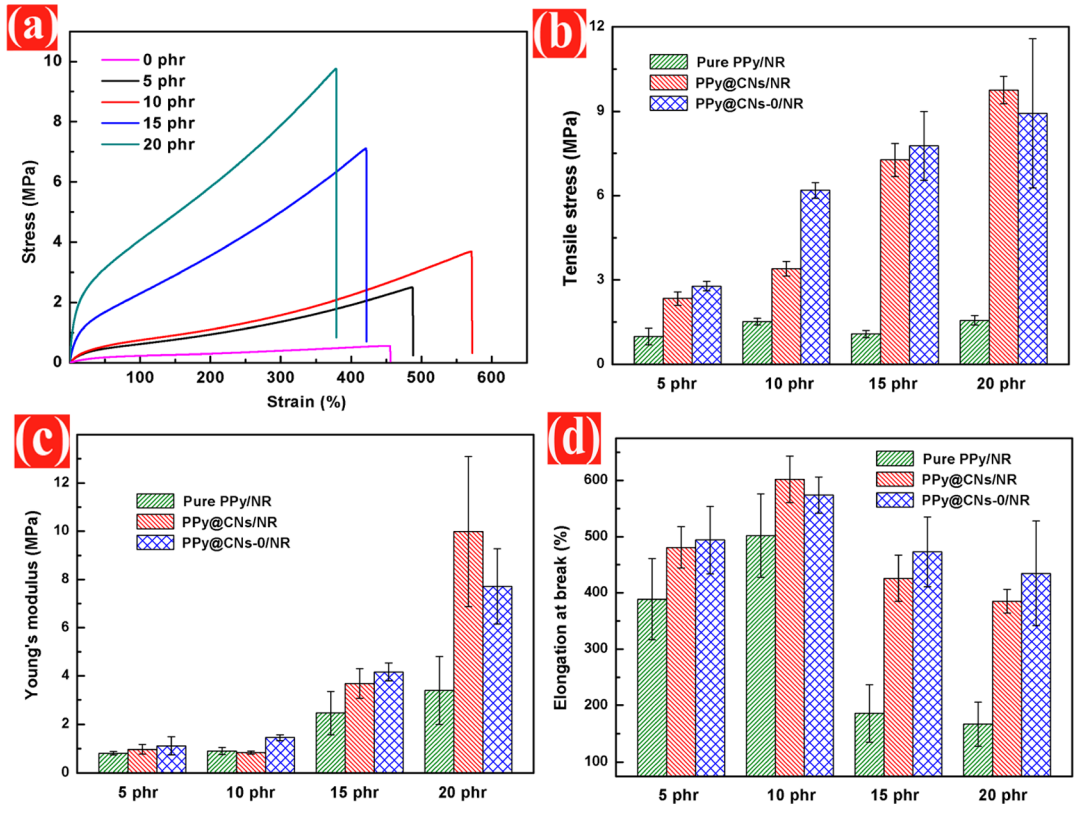

Figure 8. Stress−strain curves of PPy@CNs/NR nanocomposites with 0, 5, 10, 15, and 20 phr PPy (a); tensile stress (b), Young's modulus (c), and elongation at break (d) of PPy/NR, PPy@CNs/NR, and PPy@CNs-0/NR nanocomposites with different PPy content.

DOI: 10.1021/sc500853m
ACS Sustainable Chem. Eng. 2015, 3, 675−682

nanocomposites with nearly identical performance compared with PPy@CNs-0/NR nanocomposites makes it more suitable and applicable for the large scale application of CNs based conductive nanocomposites.

CONCLUSIONS

In summary, we have developed a sustainable, cost-effective, and scalable approach to prepare a PPy@CNs nanohybrid via a dialysis-free and in situ doping strategy. Specifically, CNs were not isolated from the hydrolysate by the water- and time-consuming dialysis process. The hydrolysis products of CNs were used without further separation as the starting materials for preparation of the PPy@CNs nanohybrid. Moreover, the synthesized PPy@CNs was in situ doped by the residual hydrolysis acid, endowing the PPy@CNs nanohybrid electrical conductivity. It was found that PPy was deposited on CNs as a continuous nodular structure, forming a PPy@CNs nanohybrid with the desired electric conductivity and adjustable dispersibility. In addition, we prepared PPy@CNs/NR nanocomposites, as well as neat PPy/NR and PPy@CNs-0/NR nanocomposites for comparison, by co-coagulation and hot-pressing. The results showed that PPy@CNs/NR nanocomposites exhibited significant improvement in electrical conductivity and mechanical properties when compared with neat PPy/NR composites, and exhibited similar performance compared with PPy@CNs-0/NR nanocomposites. This work provides a new strategy to realize the facile and environmentally friendly production of a PPy@CNs nanohybrid, which open up new opportunities for the large scale fabrication and application of CNs based conductive nanocomposites with low cost and high performance.

ASSOCIATED CONTENT

Supporting Information

Table of vulcanization formula for preparation of NR based nanocomposites, image of the PPy@CNs nanohybrid tablet lighting up an LED device, digital pictures along with ζ-potential of PPy@CNs nanohybrid synthesized via conventional routes, TEM images of PPy@CNs nanohybrid synthesized via conventional routes. This material is available free of charge via the Internet at http://pubs.acs.org.

AUTHOR INFORMATION

Corresponding Authors

*Xinxing Zhang. E-mail: xxzwwh@scu.edu.cn. Tel: +86-28-85460607. Fax: +86-28-85402465.

*Canhui Lu. E-mail: canhuilu@263.net. Tel: +86-28-85460607. Fax: +86-28-85402465.

Author Contributions

†These authors contributed equally to this work.

Notes

The authors declare no competing financial interest.

ACKNOWLEDGMENTS

The authors thank the National Science Foundation of China (51203105 and 51473100) for financial support.

REFERENCES

(1) Hosoda, N.; Tsujimoto, T.; Uyama, H. Green composite of poly(3-hydroxybutyrate-co-3-hydroxyhexanoate) reinforced with porous cellulose. *ACS Sustainable Chem. Eng.* **2014**, *2* (2), 248−253.

(2) Boissou, F.; Vigier, K. D. O.; Estrine, B.; Marinkovic, S.; Jérôme, F. Selective depolymerization of cellulose to low molecular weight cello-oligomers catalyzed by betaïne hydrochloride. *ACS Sustainable Chem. Eng.* **2014**, *2* (12), 2683−2689.

(3) Salam, A.; Lucia, L. A.; Jameel, H. A novel cellulose nanocrystals-based approach to improve the mechanical properties of recycled paper. *ACS Sustainable Chem. Eng.* **2013**, *1* (12), 1584−1592.

(4) Lam, E.; Leung, A. C. W.; Liu, Y.; Majid, E.; Hrapovic, S.; Male, K. B.; Luong, J. H. T. Green strategy guided by raman spectroscopy for the synthesis of ammonium carboxylated nanocrystalline cellulose and the recovery of byproducts. *ACS Sustainable Chem. Eng.* **2013**, *1* (2), 278−283.

(5) Yanamala, N.; Farcas, M. T.; Hatfield, M. K.; Kisin, E. R.; Kagan, V. E.; Geraci, C. L.; Shvedova, A. A. In vivo evaluation of the pulmonary toxicity of cellulose nanocrystals: A renewable and sustainable nanomaterial of the future. *ACS Sustainable Chem. Eng.* **2014**, *2* (7), 1691−1698.

(6) Wu, X. D.; Lu, C. H.; Zhang, W.; Yuan, G. P.; Xiong, R.; Zhang, X. X. A novel reagentless approach for synthesizing cellulose nanocrystal-supported palladium nanoparticles with enhanced catalytic performance. *J. Mater. Chem. A* **2013**, *1*, 8645−8652.

(7) Benaissi, K.; Johnson, L.; Walsh, D. A.; Thielemans, W. Synthesis of platinum nanoparticles using cellulosic reducing agents. *Green Chem.* **2010**, *12*, 220−222.

(8) Rezayat, M.; Blundell, R. K.; Camp, J. E.; Walsh, D. A.; Thielemans, W. Green one-step synthesis of catalytically active palladium nanoparticles supported on cellulose nanocrystals. *ACS Sustainable Chem. Eng.* **2014**, *2* (5), 1241−1250.

(9) Zhou, Z. H.; Lu, C. H.; Wu, X. D.; Zhang, X. X. Cellulose nanocrystals as a novel support for CuO nanoparticles catalysts: Facile synthesis and their application to 4-nitrophenol reduction. *RSC Adv.* **2013**, *3*, 26066−26073.

(10) Mukherjee, S. M.; Woods, H. J. X-ray and electron microscope studies of the degradation of cellulose by sulphuric acid. *Biochim. Biophys. Acta* **1953**, *10*, 499−511.

(11) Nyström, G.; Mihranyan, A.; Razaq, A.; Lindström, T.; Nyholm, L.; Strømme, M. A nanocellulose polypyrrole composite based on microfibrillated cellulose from wood. *J. Phys. Chem. B* **2010**, *114* (12), 4178−4182.

(12) Wu, X. Y.; Tang, J. T.; Duan, Y. C.; Yu, A. P.; Berry, R. M.; Tam, K. C. Conductive cellulose nanocrystals with high cycling stability for supercapacitor applications. *J. Mater. Chem. A* **2014**, *2*, 19268−19274.

(13) Wu, X. Y.; Chabot, V. L.; Kim, B. K.; Yu, A. P.; Berry, R. M.; Tam, K. C. Cost-effective and scalable chemical synthesis of conductive cellulose nanocrystals for high-performance supercapacitors. *Electrochim. Acta* **2014**, *138* (20), 139−147.

(14) Liew, S. Y.; Thielemans, W.; Walsh, D. A. Electrochemical capacitance of nanocomposites polypyrrole/cellulose films. *J. Phys. Chem. C* **2010**, *114* (41), 17926−17933.

(15) Wang, Z. H.; Tammela, P.; Zhang, P.; Huo, J. X.; Ericson, F.; Strømme, M.; Nyholm, L. Freestanding nanocellulose-compositefibre reinforced 3D polypyrrole electrodes for energy storage applications. *Nanoscale* **2014**, *6*, 13068−13075.

(16) Ferraz, N.; Strømme, M.; Fellström, B.; Pradhan, S.; Nyholm, L.; Mihranyan, A. In vitro and in vivo toxicity of rinsed and aged nanocellulose−polypyrrole composites. *J. Biomed. Mater. Res., Part A* **2012**, *100A* (8), 2128−2138.

(17) Liu, D. Y.; Sui, G. X.; Bhattacharyya, D. Synthesis and characterisation of nanocellulose-based polyaniline conducting films. *Compos. Sci. Technol.* **2014**, *99* (30), 31−36.

(18) Tang, J. T.; Song, Y.; Berry, R. M.; Tam, K. C. Polyrhodanine coated cellulose nanocrystals as optical pH indicators. *RSC Adv.* **2014**, *4*, 60249−60252.

(19) Wu, X. D.; Lu, C. L.; Xu, H. Y.; Zhang, X. X.; Zhou, Z. H. Biotemplate synthesis of polyaniline@cellulose nanowhiskers/natural rubber nanocomposites with 3D hierarchical multiscale structure and improved electrical conductivity. *ACS Appl. Mater. Interfaces* **2014**, *6* (23), 21078−21085.

DOI: 10.1021/sc500853m
ACS Sustainable Chem. Eng. 2015, 3, 675−682

(20) Cabuk, M.; Alan, Y.; Yavuz, M.; Unal, H. I. Synthesis, characterization and antimicrobial activity of biodegradable conducting polypyrrole-graft-chitosan copolymer. *Appl. Surf. Sci.* **2014**, *318* (1), 168−175.
(21) Tang, L.; Han, J. L.; Jiang, Z. L.; Chen, S. Y.; Wang, H. P. Flexible conductive polypyrrole nanocomposite membranes based on bacterial cellulose with amphiphobicity. *Carbohydr. Polym.* **2015**, *117* (6), 230−235.
(22) Huang, J. L.; Li, C. J.; Gray, D. G. Cellulose nanocrystals incorporating fluorescent methylcoumarin groups. *ACS Sustainable Chem. Eng.* **2013**, *1* (9), 1160−1164.
(23) Feng, J. T.; Li, J. J.; Lv, W.; Xu, H.; Yang, H. H.; Yan, W. Synthesis of polypyrrole nano-fibers with hierarchical structure and its adsorption property of Acid Red G from aqueous solution. *Synth. Met.* **2014**, *191*, 66−73.
(24) Zhou, Z. H.; Zhang, X. X.; Lu, C. H.; Lan, L. D.; Yuan, G. P. Polyaniline-decorated cellulose aerogel nanocomposite with strong interfacial adhesion and enhanced photocatalytic activity. *RSC Adv.* **2014**, *4*, 8966−8972.
(25) Dar, M. A.; Kotnala, R. K.; Verma, V.; Shah, J.; Siddiqui, W. A.; Alam, M. High magneto-crystalline anisotropic core-shell structured $Mn_{0.5}Zn_{0.5}Fe_2O_4$/polyaniline nanocomposites prepared by in situ emulsion polymerization. *J. Phys. Chem. C* **2012**, *116* (9), 5277−5287.
(26) Gedela, V. R.; Srikanth, V. V. Electrochemically active polyaniline nanofibers (PANi NFs) coated grapheme nanosheets/PANi NFs composite coated on different flexible substrates. *Synth. Met.* **2014**, *193*, 71−76.
(27) Joulazadeh, M.; Navarchian, A. H. Polypyrrole nanotubes versus nanofibers: A proposed mechanism for predicting the final morphology. *Synth. Met.* **2015**, *199*, 37−44.
(28) Xu, X. Z.; Liu, F.; Jiang, L.; Zhu, J. Y.; Haagenson, D.; Wiesenborn, D. P. Cellulose nanocrystals vs. cellulose nanofibrils: a comparative study on their microstructures and effects as polymer reinforcing agents. *ACS Appl. Mater. Interfaces* **2013**, *5* (8), 2999−3009.
(29) Yao, X. L.; Qi, X. D.; He, Y. L.; Tan, D. S.; Chen, F.; Fu, Q. Simultaneous reinforcing and toughening of polyurethane via grafting on the surface of microfibrillated cellulose. *ACS Appl. Mater. Interfaces* **2014**, *6* (4), 2497−2507.

DOI: 10.1021/sc500853m
ACS Sustainable Chem. Eng. 2015, 3, 675−682